Theoretical and Applied Fracture Mechanics 120 (2022) 103392

Contents lists available at ScienceDirect

Theoretical and Applied Fracture Mechanics

journal homepage: www.elsevier.com/locate/tafmec

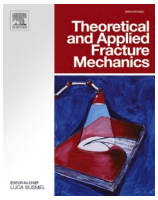

Ultra-low cycle fatigue (ULCF) in fibre-reinforced concrete beams

Federico Accornero [a,*], Alessio Rubino [a], Alberto Carpinteri [a,b]

[a] Dept of Structural, Geotechnical and Building Engineering, Politecnico di Torino, Torino, Italy
[b] Zhujiang (Pearl River) Professor of Guangdong Province, Dept of Civil and Environmental Engineering, Shantou University, Shantou, PR China

ARTICLE INFO

Keywords:
Fibre-reinforced concrete
Ultra-low cycle fatigue
Updated Bridged Crack Model
Constitutive laws
Hysteretic behaviour

ABSTRACT

Civil structures subjected to extreme loading conditions, e.g., earthquakes, undergo large deformations and fracture due to ultra-low cycle fatigue (ULCF). Although several efforts have been made to understand and to model monotonic damage and low-cycle fatigue, so far ULCF is neither sufficiently investigated nor understood. In the present work, ULCF of fibre-reinforced concrete (FRC) beams subjected to bending is discussed in the framework of Fracture Mechanics by means of the Updated Bridged Crack Model (UBCM). The model focuses on the evolution of the fracturing process at the critical cross-section of the beam, taking into account the loading reversal. The concrete matrix is assumed to be linear-elastic and perfectly-brittle. On the other hand, the toughening contribution of the reinforcing fibres is described by a constitutive law that defines the hysteretic behaviour at the single fibre level. The suitability of the hysteretic constitutive law is discussed on the basis of experimental results recently reported in the current scientific literature, in which ULCF flexural tests were carried out on FRC specimens.

1. Introduction

During the last few decades, an increasing attention has been paid to understand the main variables affecting the flexural behaviour of fibre-reinforced concrete (FRC) specimens, when they are subjected to monotonically increasing flexural loadings. In this context, a large amount of research work, both theoretical and experimental, made it clear that the flexural performance depends on several parameters: (i) the fibre volume fraction, V_f [1–10]; (ii) the mechanical and geometrical properties of the reinforcing fibres (tensile strength, geometric profile, and aspect ratio) and of the cementitious matrix (generally connected to its compression strength) [11–14]; (iii) the specimen sizes [15–18]; (iv) the fibre distribution within the volume of the composite [19].

At the same time, several investigations can be found in the current scientific literature if cyclic loading is considered. Most of them are focused on the flexural behaviour of FRC specimens subjected to high-cycle fatigue, in which the performance of the composite is interpreted by means of a Wöhler-type approach, leading to the evaluation of the fatigue life as a function of the applied stress range (*S-N* curve). This approach focuses on the sub-critical crack growth that leads to the final failure of the structural element [20,21]. In this framework, several Authors investigated the fatigue capacity of FRC specimens subjected to tensile [22–24] or flexural cyclic loading [25–35], reporting that the presence of reinforcing fibres provides a better fatigue performance of the FRC component, with respect to the plain concrete.

Nevertheless, it should be noted that this condition is far from that usually recurring in civil structural engineering applications, where the FRC members are required to provide a large energy dissipation under a low number of loading cycles due to the seismic action. For this purpose, just few experimental works can be found in the current literature [36–37] and no theoretical and analytical model is provided.

In the present paper, the Bridged Crack Model is proposed as a fracture mechanics based approach, which is able to describe the flexural behaviour of FRC beams subjected to ultra-low cycle fatigue (ULCF), i.e., when the number of loading cycles is approximately smaller than 100. This number of cycles is generally identified as the one bridging the gap between the static failure of a structure and its regime of low-cycle fatigue (LCF). As it will be shown in the following, the present work focuses on the evaluation of the hysteretic behaviour of the FRC structural element when different testing conditions are imposed, rather than the assessment of the fatigue life of the composite structure (number of cycles required to its failure).

The Bridged Crack Model, originally proposed for steel-bar reinforced concrete elements [38–40], and then extended to the case of a large number of reinforcement layers [41–48], has been recently adapted by the authors to the case of FRC elements subjected to

* Corresponding author.
E-mail address: federico.accornero@polito.it (F. Accornero).

https://doi.org/10.1016/j.tafmec.2022.103392
Received 17 November 2021; Received in revised form 17 March 2022; Accepted 10 May 2022
Available online 20 May 2022

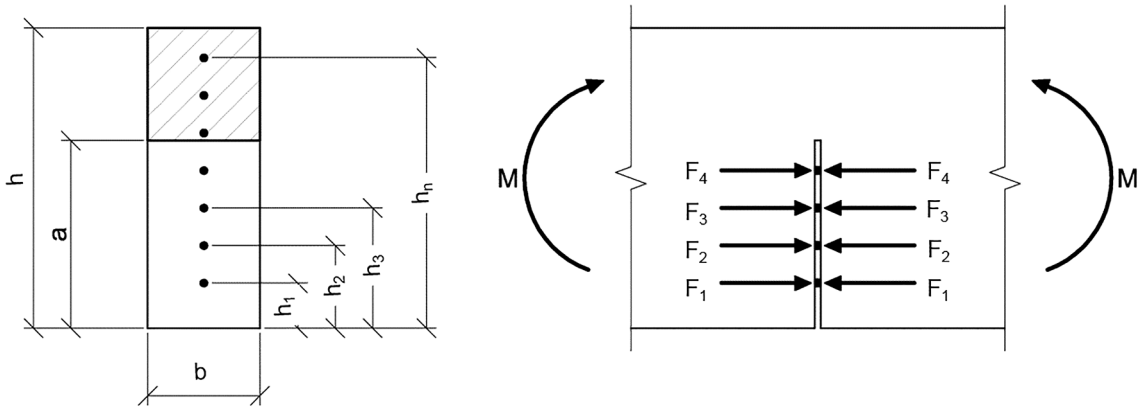

Fig. 1. Fibre-reinforced brittle-matrix beam model.

monotonically increasing flexural loadings [49,50]. A further extension to the case of FRC members subjected to ULCF is discussed herein by proposing a new constitutive law that describes the hysteresis at the single fibre level. In the following sections, the model is extensively discussed and the suitability of the hysteretic constitutive law herein proposed is validated on the basis of experimental results reported in the scientific literature [36].

2. The Updated Bridged Crack Model (UBCM)

2.1. Fundamentals

Considering a FRC beam element subjected to flexural loading, the model is able to describe the evolution of the fracturing process occurring in a notched or unnotched rectangular cross-section where the damage is localized. The cross-section is geometrically characterized by the thickness, b, the depth, h, the initial notch depth, a_0, and it is subjected to an external bending moment, M (Fig. 1).

The total number of fibres in the cross-section, n, is calculated as:

$$n = \alpha V_f \frac{bh}{A_f}, \tag{1}$$

where A_f is the cross-sectional area of the single fibre, and α the orientation factor [51]. The $m < n$ fibres crossing the actual crack are considered as active and their bridging action is taken into account by the closing forces, F_i, calculated as:

$$F_i = \beta_i \sigma_s A_f, \tag{2}$$

in which σ_s is the nominal stress in the i-th reinforcing fibre adjusted by a coefficient β_i, which includes other phenomena as the "group effect" and the "snubbing effect" [52].

On the left of Fig. 2, a schematic of the notched cross-section subjected to bending is reported. Experimental evidences lead to identify the following four regions within the cross-section: (i) ligament in compression; (ii) uncracked ligament in tension; (iii) fibre bridging zone, in which the reinforcing fibres bridge the crack; (iv) stress-free crack zone —generally noticeable for large crack depths or very short fibres— where the bridging action of the fibres has vanished.

These regions can be effectively interpreted by the Updated Bridged Crack Model (UBCM). The model assumes the composite as a bi-phase material, in which the brittle matrix and the reinforcing fibres represent its primary and secondary phases, both contributing to the global toughness of the structural material. The matrix is assumed to be elastic-perfectly brittle, other nonlinear contributions being neglected. On the other hand, the bridging mechanism of the secondary phase can be described by an appropriate cohesive softening constitutive law, which takes into account: (i) the progressive slippage of the fibre inside the matrix, when the external load tends to open the crack; (ii) the contrasting action of the fibres against the crack closure, in the case of loading reversal. In both cases, i.e., monotonically increasing and cyclic loading, the corresponding constitutive laws will be defined in the following.

Under these assumptions, a singular stress distribution is predicted at the crack tip (see Fig. 2) in agreement with Linear Elastic Fracture Mechanics (LEFM) concepts, the matrix toughening contribution being defined by its fracture toughness, K_{IC}. Thus, the singular crack-tip stress

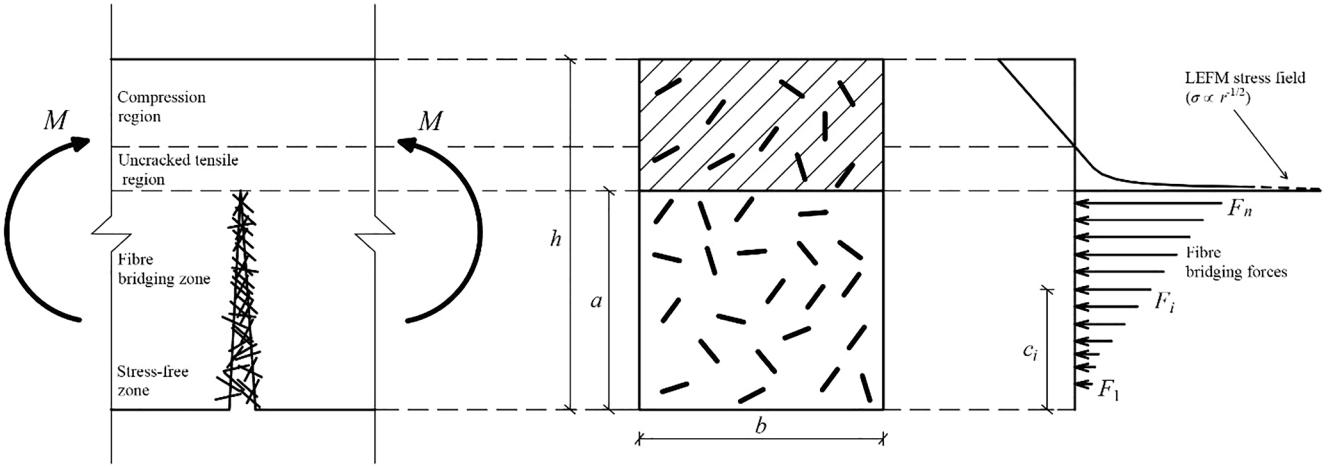

Fig. 2. Critical cross-section in a FRC beam with the stress distribution predicted by the UBCM.

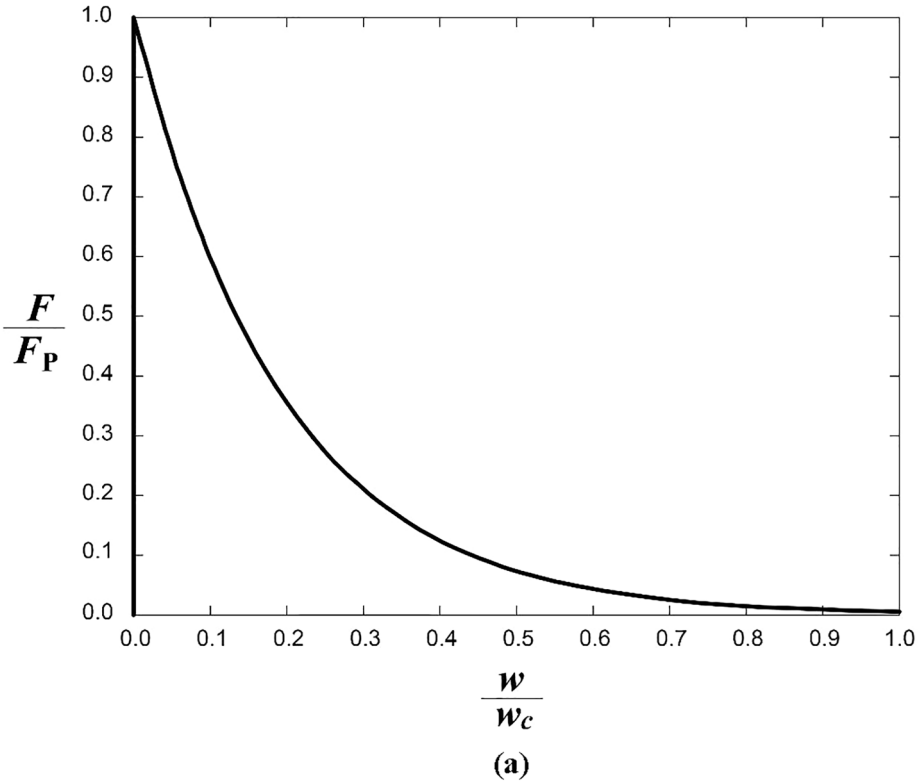

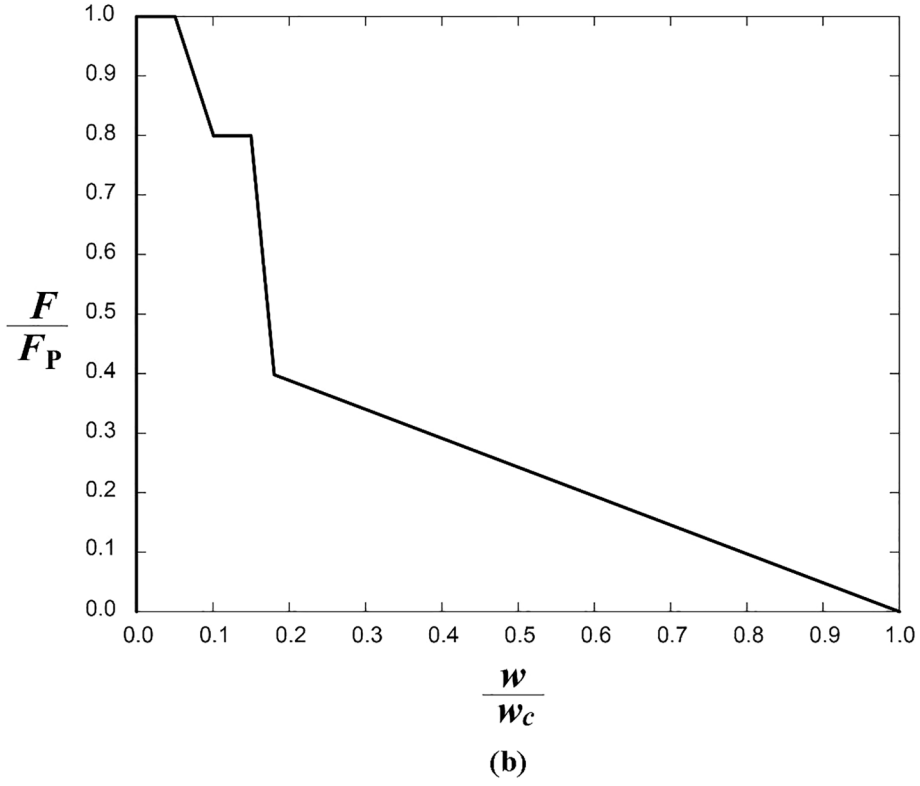

Fig. 3. Slippage law per unit embedded length: **(a)** Straight fibre; **(b)** Hooked-end fibre.

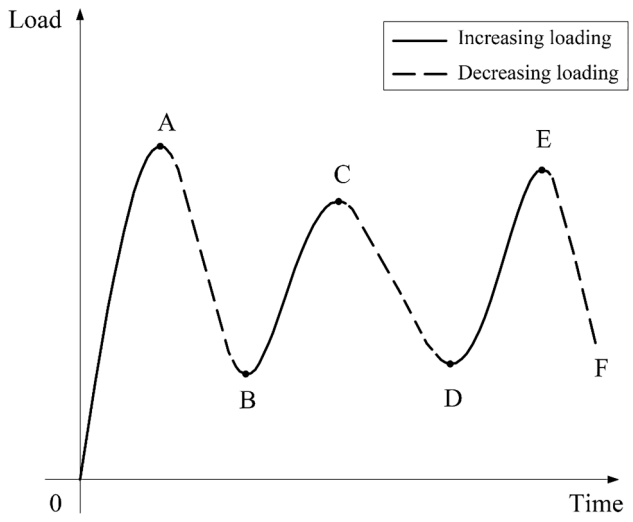

Fig. 4. Decomposition of the loading history into monotonic paths.

field is uniquely characterized by a global stress-intensity factor, K_I:

$$K_I = K_{IM} - \sum_{i=1}^{m} K_{Ii} = \frac{M}{bh^{3/2}} Y_M - \frac{\{Y_F\}^T\{F\}}{bh^{1/2}}, \tag{3}$$

in which the contributions related to the applied bending moment, K_{IM}, and to the i-th reinforcing fibre, K_{Ii}, appear. In agreement with LEFM criteria, the crack propagation occurs when the stress-intensity factor, K_I, reaches its critical value, K_{IC}, i.e., the fracture toughness of the plain matrix (unreinforced material).

2.2. Monotonically increasing load

During a typical experimental flexural test, the external bending moment tends continuously to widen the crack until the complete disconnection of the FRC specimen. This phenomenon is tackled by the reinforcing fibres, which provide a bridging action that is a function of the slippage behaviour of the fibre inside the cementitious matrix.

The slippage behaviour of the fibre-reinforcements is typically investigated by means of pull-out tests carried out on the single fibre. Considering the extensive literature regarding this issue, it can be said that remarkable changes in the response can be observed depending on the fibre material (steel, polymer, etc.), the fibre geometry (straight, crimped, twisted, with hooked ends, etc.), the compression strength of the cementitious matrix, as well as the orientation of the fibre with respect to the direction of the pull-out load [53–54].

In this context, a significant investigation has been recently carried out by Abdallah et al. [55] on the basis of experimental pull-out tests on steel fibres. These Authors proposed a generalized pull-out law per unit embedded length of the fibre, which is valid for the case of straight and hooked ends steel fibres. These two constitutive laws are represented in Fig. 3, where the bridging force, F, is plotted as a function of the relative slip (or crack opening displacement), w, in terms of normalized coordinates. This normalization is defined by the maximum value of the bridging force, F_P, beyond which the fibre pull-out starts, and by the equivalent embedded length, w_c, representing the slip (or crack opening) beyond which the fibre is entirely pulled-out from the matrix, and therefore its bridging effect is exhausted. In addition, for the case of hooked-end steel fibres (Fig. 3b), the final branch —generally described by an exponential law— is simplified by a linear relationship. These laws have been recently implemented in the UBCM, proving their effectiveness in reproducing the flexural response of FRC members subjected to monotonically increasing flexural loadings [49,50].

In addition, a set of compatibility conditions is needed to calculate the crack opening, w_i, at each i-th active reinforcement level as a function of the applied bending moment, M, and of the m bridging forces, F_i. In matrix form, we have:

$$\{w\} = \{\lambda_M\}M - [\lambda]\{F\}, \tag{4}$$

where $\{w\}$ is the crack opening vector, $\{\lambda_M\}$ is the vector of the local compliances due to the bending moment, and $[\lambda]$ is the matrix of the local compliances due to the bridging forces.

Summarizing, for a given crack depth, the problem relies in the determination of the $2m + 1$ unknowns, i.e., the fracturing moment, M_F, the profile of the crack opening displacements, $\{w\}$, and the corresponding distribution of bridging forces, $\{F\}$. The solution requires a numeric iterative procedure that leads to the complete evaluation of the stress-block diagram at cross-sectional level. By applying the routine for different values of crack depths, the model is able to fully describe the evolution of the fracturing process up to the complete disconnection of the critical cross-section ($a \sim h$), taking into account the effect of the active fibres that bridge the crack (Fig. 2).

2.3. Cyclic loading

The case of repeated loading can be easily addressed if the generic loading history is intended as the sum of consequent monotonic paths, each characterized by monotonically increasing or decreasing load (Fig. 4). Under these assumptions, the fundamentals of the model are valid for each monotonic branch of the entire loading process, as long as each initial configuration is defined (subscript zero in the following).

The key-point relies in the behaviour of the reinforcing fibres during the unloading phases of the process. In this context, it is possible to take advantage of the recent experimental results obtained by Fataar et al. [56], who investigated the static and fatigue behaviour of hooked-end steel fibres.

Regarding the fatigue life of the fibre, a certain scatter was observed in the experimental results due to the different failure mechanisms (fibre rupture or fibre pull-out) that can occur depending on the applied load level and on the amount of pre-slip. Besides this statistical deviation, which typically characterizes the pull-out tests of short fibres, and considering the fatigue pull-out load vs displacement curve, it can be found that: (i) the static pull-out curve represents an envelope of the fatigue pull-out curves; (ii) during the unloading phase, the behaviour is described by a vertical branch, i.e., a rigid response of the single fibre. Nevertheless, no information can be found about the compression behaviour of the single fibre because fatigue tests were performed in order to maintain tensile loads throughout the cycles.

On the basis of these considerations, an appropriate constitutive law at the single-fibre level has been implemented in the UBCM, which is represented in Fig. 5 for the case of hooked-end steel fibres and in terms of normalized coordinates. The continuous line refers to the case of monotonically increasing loading, in which the fibre opposes to the crack opening, whereas the external bending moment tends to open the crack. On the other hand, at the onset of the unloading phase of the process, a rigid behaviour of the fibre is considered (see the vertical dashed branch of the diagram), consistently with the previous discussion. In this phase, the fibre contrasts the crack closure, keeping unchanged the crack opening at the reinforcement level. This behaviour is assumed to be valid also in the case of compressive regime of the fibre, until the maximum compressive force, which is assumed equal to $-F_P$, is reached. The latter is intended as the compression force required to activate the reversal of the fibre slippage and the consequent decrease in the crack opening. In this phase, a plastic behaviour of the fibre is assumed (see the horizontal plateau), which is valid until the load starts to increase again (see the vertical dotted branch). In this way, the hysteretic dissipation at the single fibre level is completely defined (see the shaded grey area).

For each phase of the loading process, the crack propagation condition is still defined by Eq. (3). The corresponding compatibility

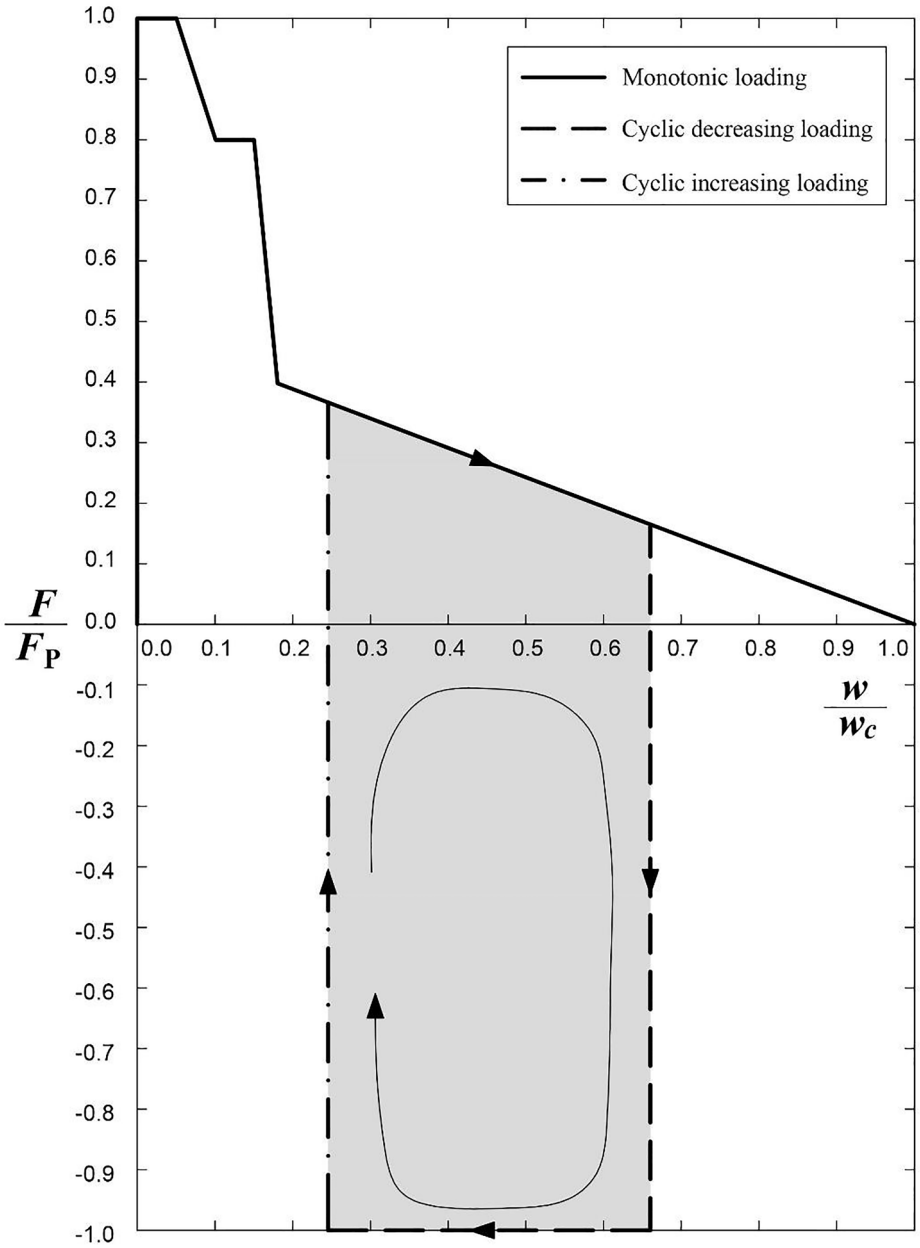

Fig. 5. Hysteretic behaviour at the single-fibre level.

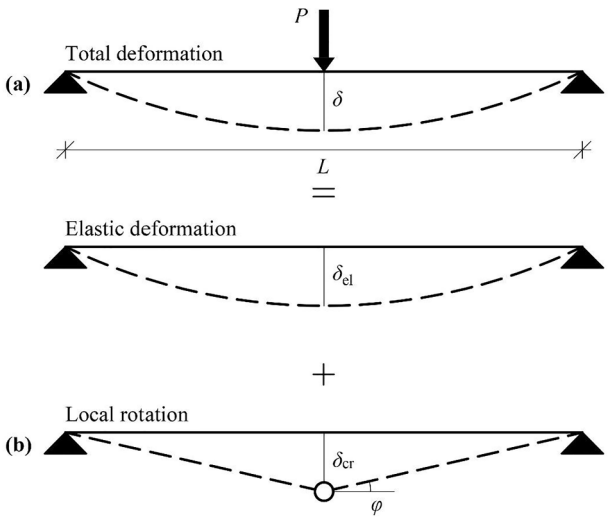

Fig. 6. Superposition principle of elastic deflection and local rotation of the beam.

conditions are obtained by rewriting Eq. (4) in the incremental form:

$$\{w\} - \{w_0\} = \{\lambda_M\}(M - M_0) - [\lambda](\{F\} - \{F_0\}), \tag{5}$$

where the quantities $\{w_0\}$, M_0, and $\{F_0\}$ describe the initial configuration of the cracked cross-section due to the previous phases of the loading process.

Analogously to the monotonic case, the unknowns of the problem (M_F, $\{w\}$, $\{F\}$) are obtained by a numerical iterative procedure.

2.4. Mechanical response of the FRC cross-section

When the stress-block diagram is evaluated for a given crack depth, the local rotation of the notched cross-section can be calculated in the case of monotonic loading:

$$\varphi = \lambda_{MM} M - \{\lambda_M\}^T \{F\}, \tag{6}$$

or in the case of cyclic regime:

$$\varphi - \varphi_0 = \lambda_{MM}(M - M_0) - \{\lambda_M\}^T(\{F\} - \{F_0\}) \tag{7}$$

In both cases, the corresponding deflection δ of the FRC element can be obtained by applying the superposition principle, according to which the total deflection takes into account both the inelastic contribution related to the fracturing process in the mid-span section (inelastic hinge) and that related to the elastic behaviour of the remaining part of the beam. In Fig. 6, the application of the superposition principle is schematically shown in the case of a three-point bending test.

Under these assumptions, the UBCM predicts different post-cracking regimes as a function of two scale-dependent dimensionless numbers, i.e., the *reinforcement brittleness number*, N_P, and the *pull-out brittleness number*, N_w [49,50]:

$$N_P = \frac{\sum_{i=1}^{n} F_{P,i}}{K_{IC} b h^{1/2}} = V_f \frac{\alpha \bar{\beta} \sigma_{s,max}}{K_{IC}} h^{1/2} = V_f \frac{\overline{\sigma}_{s,max}}{K_{IC}} h^{1/2}, \tag{8}$$

$$N_w = \frac{E w_c}{K_{IC} h^{1/2}}. \tag{9}$$

As recently discussed by the authors [49,50], the *reinforcement brittleness number*, N_P, is directly connected to the load bearing capacity of the FRC specimen. It depends on the fibre volume fraction, V_f, on the maximum value of the generalized tensile stress acting in the reinforcing fibre, $\overline{\sigma}_{s,max}$ —in which the parameters of fibre distribution, α and β, are included— on the matrix fracture toughness, K_{IC}, as well as on the beam depth, h.

On the other hand, the *pull-out brittleness number*, N_w, governs the exhaustion of the fibre toughening action, defining in this way the softening tail of the load–deflection curve and the inelastic rotation capacity of the FRC cross-section. It depends on the matrix Young's modulus, E, on the equivalent (average) embedded length of the fibre, w_c, on the matrix fracture toughness, K_{IC}, and on the beam depth, h.

It is worth emphasizing that the coefficients related to the fibre distribution, i.e., the orientation factor, α, which affects the number of fibres crossing the critical cross-section (Eq. (1)), and the coefficient β_i, which takes into account the orientation of the fibre during its pull-out (Eq. (2)), are included in the generalized slippage strength of the fibre, $\overline{\sigma}_{s,max}$, and thus in N_P. As it will be shown in the following, the identification of $\overline{\sigma}_{s,max}$ on the basis of experimental flexural tests permits to

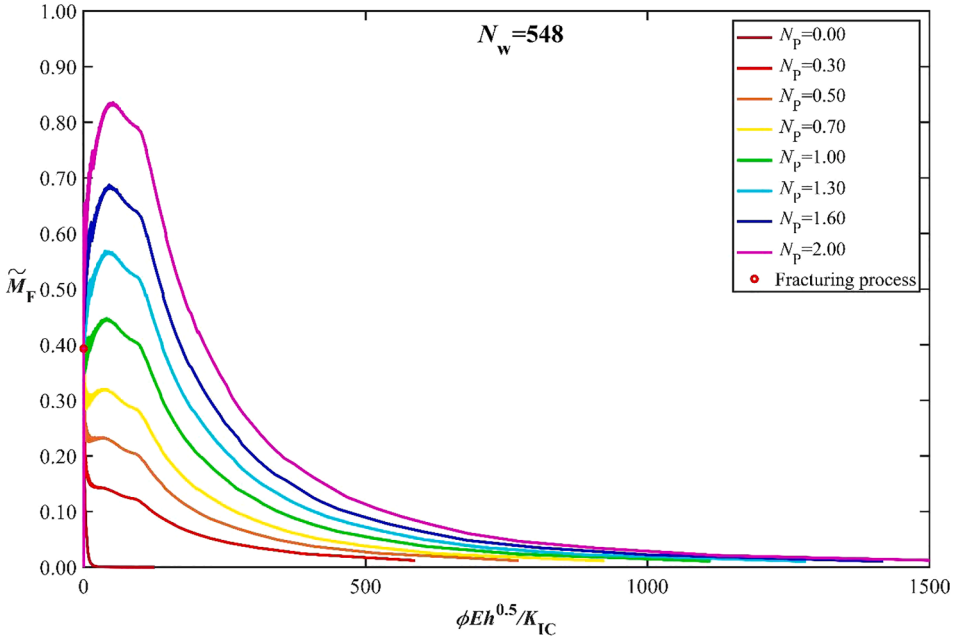

Fig. 7. Structural response of FRC beams ($a_0/h = 0.05$) by varying N_P, for a given value of N_w.

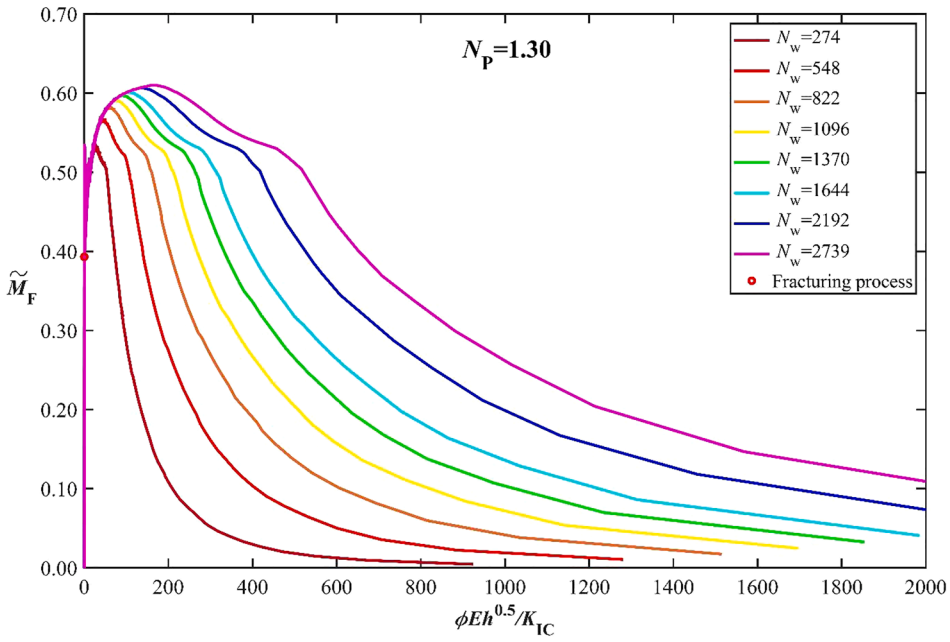

Fig. 8. Structural response of FRC beams ($a_0/h = 0.05$) by varying N_w, for a given value of N_P.

predict the flexural response of the composite, thus incorporating the information related to the fibre distribution without any determination of the single values of α and β_i.

3. Influence of N_P and N_w

In this section, some numerical analyses are shown in order to describe the influence of the two brittleness numbers, N_P and N_w, on the post-cracking response of FRC beams. In all cases, the response of the notched rectangular cross-section ($a_0/h = 0.05$) is described in terms of dimensionless fracturing moment vs local rotation diagrams.

In Fig. 7, the numerical curves are plotted for a constant value of N_w equal to 548, whereas N_P ranges from 0 (unreinforced material) to 2. It can be observed that N_P drives a ductile-to-brittle transition in the post-cracking response of the composite. As already discussed by the authors [47,50], the critical value of the *reinforcement brittleness number*, N_{PC}, permits to define the minimum (critical) fibre volume fraction, $V_{f,min}$, or, equivalently, the minimum (critical) specimen size, h_{min}, required to guarantee a stable post-cracking response.

Nevertheless, it should be noted that the influence of N_P is restricted to the second stage of the response, in which the load bearing capacity of the FRC cross-section can be evaluated. This restriction is due to the influence of N_w, which drives the final decrement of the carried load, providing the convergence of all the curves to a unique final softening tail (Fig. 8).

In Fig. 8, the family of curves is plotted for a constant value of N_P equal to 1.30, whereas N_w ranges from 274 to 2739. Consistently with the previous considerations, a pseudo-hardening post-cracking response is observed in all cases, being N_P greater that N_{PC}. Then, the numerical curves split towards different final softening branches depending on the value of N_w, which defines the inelastic rotation capacity of the FRC cross-section.

4. Experimental validation

In this section, the UBCM is used to reproduce experimental results obtained by Boulekbache et al. [36], regarding the ULCF behaviour of FRC beams. The investigation was carried out by means of four-point bending tests on prismatic notched FRC specimens characterized by a length of 700 mm (span of 600 mm), and a thickness and a depth of 150 mm. A notch of 10 mm depth was introduced in the mid-span cross-section, as schematically represented in Fig. 9.

Different variables were taken into account in the experimental program: (i) three types of cementitious matrix, including normal-

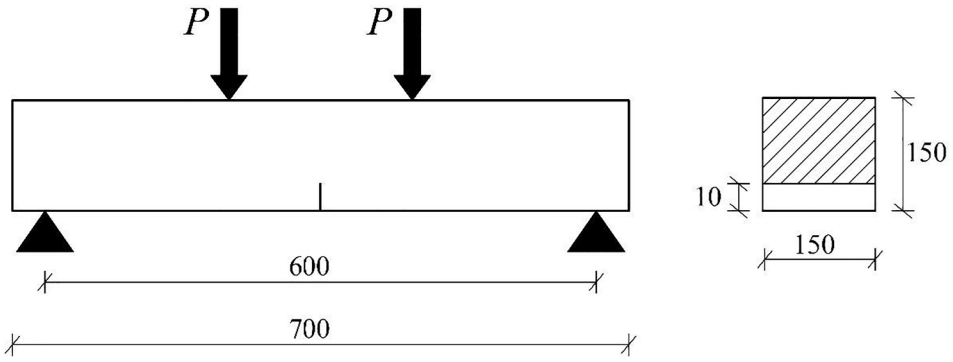

Fig. 9. Test geometry [36].

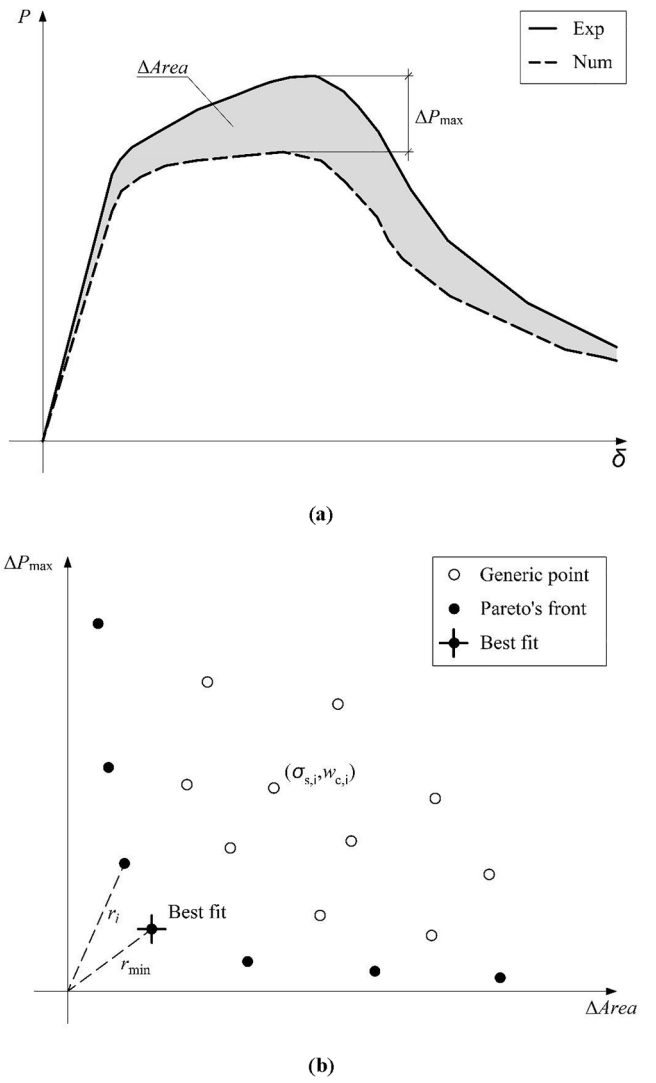

Fig. 10. **(a)** Schematic representation of ΔP_{max} and $\Delta Area$; **(b)** Multi-objective optimization following the Pareto's procedure.

strength concrete (OC), self-compacting concrete (SCC), and high-strength concrete (HSC). The mixtures were characterized by a 28-days average cubic compression strength of 29.3 MPa, 61.3 MPa, and 82.6 MPa, respectively; (ii) two types of hooked-end steel fibres, characterized by the same tensile strength, f_u, equal to 1100 MPa, but different lengths, l_f, (35 mm and 60 mm) and aspect ratios, λ (65 and 80); (iii) two fibre volume contents, equal to 0.50% and 1.00%. Further information about the composition and the mechanical properties of the composite mixture can be found in [36].

As a consequence, a total of 12 ULCF tests were performed. In this work, only the results related to the fibre with $\lambda = 65$ will be presented, since similar conclusions can be drawn in the case of $\lambda = 80$.

For each one of the six mixtures, an identification procedure is needed in order to characterize the mechanical parameters of the matrix and of the reinforcing fibres, i.e., K_{IC}, $\overline{\sigma}_{s,max}$, and w_c, which cannot be known *a priori*.

The matrix fracture toughness, K_{IC}, is determined as the first parameter, being related to the first cracking moment of the FRC specimen. In other words, K_{IC} is found by optimizing the difference between the first cracking moment experienced by the specimen and that predicted by the numerical model.

Table 1
Mechanical parameters obtained by identification and dimensionless numbers.

ID	V_f (%)	K_{IC} (MPa mm$^{1/2}$)	$\overline{\sigma}_{s,max}$ (MPa)	w_c (mm)	N_P (-)	N_w (-)
FROC 65–0.5	0.50	17	300	17.5	1.08	2475
FROC 65–1	1.00	15	233	16.5	1.90	2636
FRSCC 65–0.5	0.50	17	315	14.7	1.13	2634
FRSCC 65–1	1.00	21	287	16.8	1.67	2437
FRHSC 65–0.5	0.50	15	333	7.7	1.36	1723
FRHSC 65–1	1.00	17	379	7.0	2.73	1382

On the other hand, the other two parameters, $\overline{\sigma}_{s,max}$ and w_c, relate to the post-cracking behaviour of the composite, being directly connected to the brittleness numbers N_P and N_w. In this case, $\overline{\sigma}_{s,max}$ and w_c have been selected by taking into account two parameters: the maximum load and the area under the load vs deflection curve. For each pair of values ($\overline{\sigma}_{s,max}$, w_c), the comparison between the experimental curve and the related numerical prediction leads to evaluate the differences in terms of maximum load (ΔP_{max}) and of area under the curve ($\Delta Area$), as schematically shown in Fig. 10a.

Following Pareto's approach for the multi-objective optimization, the best-fitting solution has been chosen among the points within Pareto's front as the one with the minimum distance from the origin (Fig. 10b).

Thus, it is possible to obtain a set of three identifying parameters (K_{IC}, $\overline{\sigma}_{s,max}$, w_c) for each experimental curve, together with the corresponding brittleness numbers N_P and N_w (Table 1). It is worth noting that the parameter $\overline{\sigma}_{s,max}$ includes also the values of the orientation factor, α, which were also reported in the referenced paper [36]. The results are represented in Fig. 11 where, for each specimen series, the experimental curve is depicted together with the corresponding numerical one.

When the mechanical parameters of the composite are obtained, the ULCF behaviour of the FRC specimens can be predicted by defining the boundary conditions for each hysteretic cycle. More precisely, each loop is characterized by its maximum and minimum values in applied load and specimen deflection. The superposition between experimental data (dotted curves) and numerical predictions (continuous curves) is represented in Fig. 12 for each specimen series, showing the effectiveness of the UBCM. A consistent reproduction of the experimental curves is provided, both in terms of global response and hysteretic behaviour. It is shown that an increase in fibre volume fraction, with a correspondent increase in N_P (see Table 1), provides a more stable post-peak response of the specimen. The reinforcement brittleness number varies from 1.08 to 1.90 in the case of FROC, from 1.13 to 1.67 in the case of FRSCC, and from 1.36 to 2.73 in the case of FRHSC. In all cases, N_P is greater than its critical value, showing a pseudo-hardening global response of the composite.

Regarding the hysteretic behaviour, a consistent prediction of each single loop can be obtained, together with the corresponding dissipated energy (area bounded by the loop). In this respect, the difference between the energy dissipated during each experimental test and that predicted by the model is found to be smaller than 20%.

In addition, if we consider the slope characterizing each cycle in the P-δ diagrams, the UBCM predicts a flexural stiffness that is almost constant during the whole process. It is worth noting that, by considering a nonlinear decrease in the cycle slope, which can represent the cyclic modulus, E_{cyc} [36], it would be possible to describe the progressive matrix damaging.

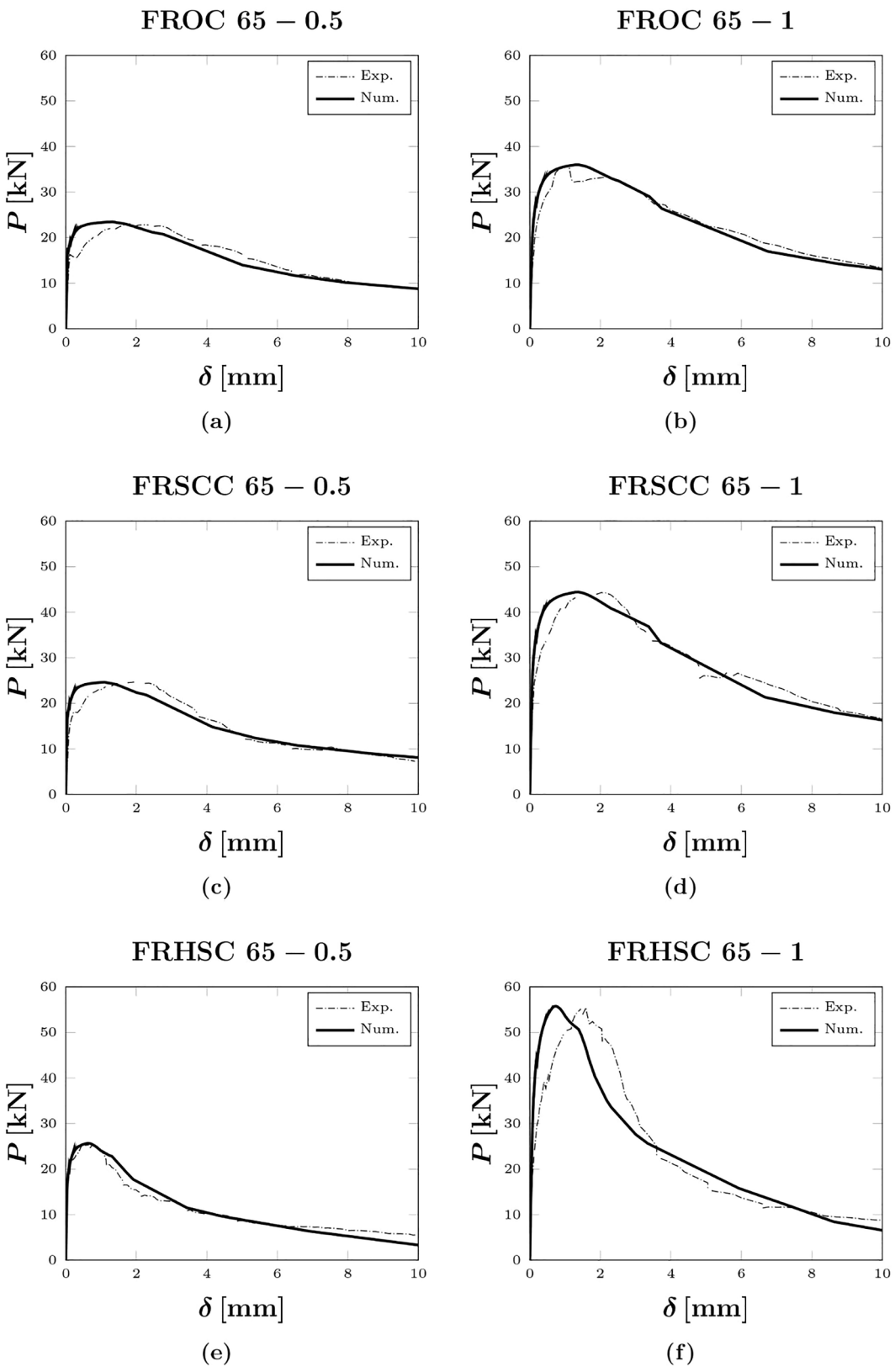

Fig. 11. Identification of the monotonic part of the experimental curves. **(a)** FROC 65–0.5; **(b)** FROC 65–1; **(c)** FRSCC 65–0.5; **(d)** FRSCC 65–1; **(e)** FRHSC 65–0.5; **(f)** FRHSC 65–1 [36].

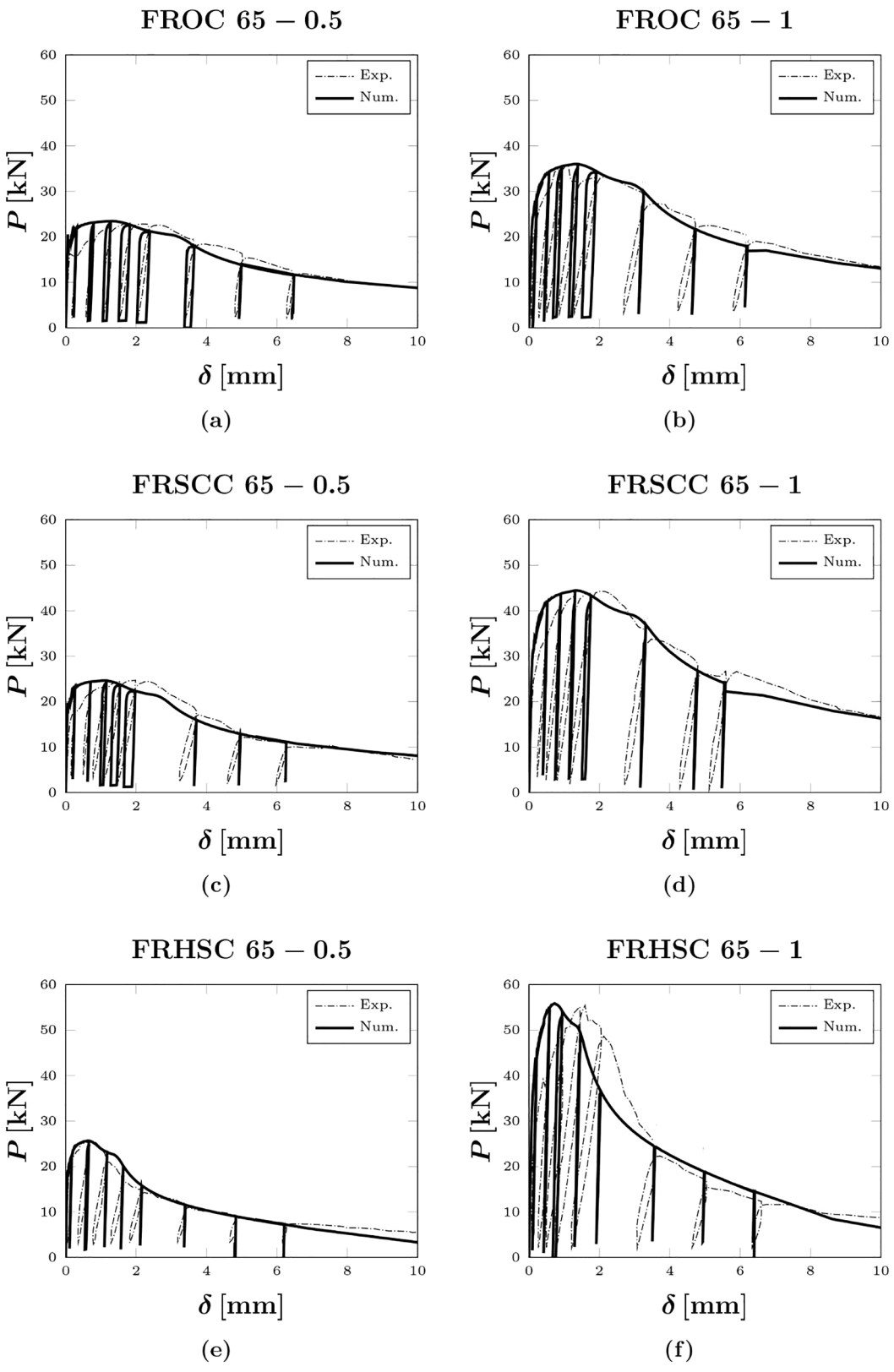

Fig. 12. Prediction of the hysteretic cycles: **(a)** FROC 65–0.5; **(b)** FROC 65–1; **(c)** FRSCC 65–0.5; **(d)** FRSCC 65–1; **(e)** FRHSC 65–0.5; **(f)** FRHSC 65–1 [36].

5. Conclusions

The Updated Bridged Crack Model (UBCM) is proposed as a Fracture Mechanics approach to interpret the behaviour of FRC beams subjected to ultra-low cycle fatigue. The model assumes the cementitious matrix as a linear-elastic perfectly-brittle phase, whereas a new σ-w constitutive law is proposed to describe the hysteretic behaviour at the single fibre level on the basis of experimental pull-out tests.

Within the model assumptions, it is possible to identify the mechanical properties of the composite phases, by taking into account the monotonic regime of the flexural response. The latter is synthetically described by two scale-dependent dimensionless numbers, N_P and N_W. Then, an effective prediction of the hysteretic response of the FRC specimens can be obtained.

The effectiveness of the model is discussed on the basis of a recent experimental campaign, in which the cyclic flexural behaviour of FRC specimens is investigated as a function of fibre volume fraction and concrete matrix. In all cases under investigation, a consistent overlapping between numerical predictions and experimental data is found, proving the suitability of the constitutive law herein proposed.

CRediT authorship contribution statement

Federico Accornero: Conceptualization, Formal analysis, Investigation, Methodology, Project administration, Validation, Writing – original draft. **Alessio Rubino:** Data curation, Software, Visualization, Writing – original draft. **Alberto Carpinteri:** Conceptualization, Funding acquisition, Methodology, Resources, Supervision, Validation, Writing – review & editing.

Declaration of Competing Interest

The authors declare that they have no known competing financial interests or personal relationships that could have appeared to influence the work reported in this paper.

References

[1] T. Almusallam, S.M. Ibrahim, Y. Al-Salloum, A. Abadel, H. Abbas, Analytical and experimental investigations on the fracture behaviour of hybrid fiber reinforced concrete, Cem. Concr. Compos. 74 (2016) 201–217, https://doi.org/10.1016/j.cemconcomp.2016.10.002.

[2] B.I.G. Barr, M.K. Lee, E.J. de Place Hansen, D. Dupont, E. Erdem, S. Schaerlaekens, B. Schnütgen, H. Stang, L. Vandewalle, Round-robin analysis of the RILEM TC 162-TDF beam-bending test: Part 1—Test method evaluation, Mat. Struct. 36 (9) (2003) 609–620.

[3] J.A.O. Barros, J.S. Cruz, Fracture energy of steel fiber-reinforced concrete, Mech. Adv. Mater. Struct 8 (1) (2001) 29–45.

[4] J.O.A. Barros, V.M.C.F. Cunha, A.F. Ribeiro, J.A.B. Antunes, Post-cracking behaviour of steel fibre reinforced concrete, Mater. Struct. 38 (1) (2005) 47–56, https://doi.org/10.1007/BF02480574.

[5] F. Bencardino, L. Rizzuti, G. Spadea, R.N. Swamy, Experimental evaluation of fiber reinforced concrete fracture properties, Compos. B Eng. 41 (1) (2010) 17–24.

[6] A.P. Fantilli, B. Chiaia, A. Gorino, Fiber volume fraction and ductility Index of concrete beams, Cem. Concr. Compos. 65 (2016) 139–149, https://doi.org/10.1016/j.cemconcomp.2015.10.019.

[7] K. Holschemacher, T. Mueller, Y. Ribakov, Effect of steel fibres on mechanical properties of high-strength concrete, Mater. Des. 31 (5) (2010) 2604–2615, https://doi.org/10.1016/j.matdes.2009.11.025.

[8] B. Mobasher, M. Bakhshi, C. Barsby, Backcalculation of residual tensile strength of regular and high performance fiber reinforced concrete from flexural tests, Constr. Build. Mater. 70 (2014) 243–253, https://doi.org/10.1016/j.conbuildmat.2014.07.037.

[9] A.E. Naaman, High Performance Fiber Reinforced Cement Composites, in: Chung DDL, ed. Vol. 1: High-Performance Construction Materials (Edited by Caijun Shi and Y L Mo) *Engineering Materials for Technological Needs*. Singapore: World Scientific Publishing Co. Pte. Ltd; 2008-91-153.

[10] T. Soetens, S. Matthys, Different methods to model the post-cracking behaviour of hooked-end steel fibre reinforced concrete, Constr. Build. Mater. 73 (2014) 458–471, https://doi.org/10.1016/j.conbuildmat.2014.09.093.

[11] S. Aydin, Effects of fiber strength on fracture characteristics of normal and high strength concrete, Periodica Polytechnica Civ. Eng. 57 (2) (2013) 191–200, https://doi.org/10.3311/PPci.7174.

[12] W.-C. Choi, K.-Y. Jung, S.-J. Jang, H.-D. Yun, The influence of steel fiber tensile strengths and aspect ratios on the fracture properties of high-strength concrete, Materials 12 (13) (2019) 2105, https://doi.org/10.3390/ma12132105.

[13] Y. Sahin, F. Koksal, The influences of matrix and steel fibre tensile strengths on the fracture energy of high-strength concrete, Constr. Build. Mater. 25 (4) (2011) 1801–1806, https://doi.org/10.1016/j.conbuildmat.2010.11.084.

[14] D.-Y. Yoo, Y.-S. Yoon, N. Banthia, Flexural response of steel-fibre-reinforced concrete beams: Effects of strength fiber content, and strain-rate, Cem. Concr. Compos. 64 (2015) 84–92, https://doi.org/10.1016/j.cemconcomp.2015.10.001.

[15] J. Flàdr, P. Bily, Specimen size effect on compressive and flexural strength of high-strength fibre-reinforced concrete containing coarse aggregate, Compos. B 138 (2018) 77–86, https://doi.org/10.1016/j.compositesb.2017.11.032.

[16] P.A. Jones, S.A. Austin, P.J. Robins, Predicting the flexural load-deflection response of steel fibre reinforced concrete from strain, crack-width, fibre pull-out and distribution data, Mater. Struct. 41 (3) (2008) 449–463, https://doi.org/10.1617/s11527-007-9327-9.

[17] S.A. Paschalis, A.P. Lampropoulos, Size effect on the flexural performance of ultra high performance fiber reinforced concrete (UHPFRC), in: Proceedings of the 7th RILEM workshop on High Performance Fiber Reinforced Cement Composites (HPFRCC-7), Stuttgart, 2015, pp. 177-184.

[18] D.-Y. Yoo, N. Banthia, J.-M. Yang, Y.-S. Yoon, Size effect in normal- and high-strength amorphous metallic and steel fiber reinforced concrete beams, Constr. Build. Mater. 121 (2016) 676–685.

[19] F. Lo Monte, L. Ferrara, Tensile behaviour identification in Ultra-High Performance Fibre Reinforced Cementitious Composites: indirect tension tests and back analysis of flexural test results, Mater Struct 53 (6) (2020).

[20] S. Invernizzi, F. Montagnoli, A. Carpinteri, Very high cycle corrosion fatigue study of the collapsed Polcevera Bridge, Italy, J. Bridge Eng. 27 (1) (2022), 04021102, https://doi.org/10.1061/(ASCE)BE.1943-5592.0001807.

[21] S. Invernizzi, F. Montagnoli, A. Carpinteri, Experimental evidence of specimen-size effects on en-aw6082 aluminum alloy in vhcf regime, Appl. Sci. 11 (9) (2021), 4272, https://doi.org/10.3390/app11094272.

[22] P. Jun, V. Mechtcherine, Behaviour of strain-hardening cement-based composites (SHCC) under monotonic and cyclic tensile loading: Part 1 – Experimental investigations, Cem. Concr. Compos. 32 (10) (2010) 801–809, https://doi.org/10.1016/j.cemconcomp.2010.07.019.

[23] S.A. Paschalis, P. Lampropoulos, Ultra-high-performance fiber-reinforced concrete under cyclic loading, ACI Mater. J. 113 (4) (2016) 419–427, https://doi.org/10.14359/51688928.

[24] N. Schäfer, V. Gudzulic, R. Breitenbücher, G. Meschke, Experimental and numerical investigation on high performance SFRC: Cyclic tensile loading and fatigue, Materials 14 (2021) 7593, https://doi.org/10.3390/ma4247593.

[25] N.K. Banjara, K. Ramanjaneyulu, Experimental investigations and numerical simulations on the flexural fatigue behavior of plain and fiber-reinforced concrete, J. Mater. Civ. Eng. (ASCE) 30 (8) (2018) 04018151, https://doi.org/10.1061/(ASCE)MT.1943-5533.0002351.

[26] D.M. Carlesso, A. de la Fuente, S.H.P. Cavalaro, Fatigue of cracked high performance fiber reinforced concrete subjected to bending, Constr. Build. Mater. 220 (2019) 444–455, https://doi.org/10.1016/j.conbuildmat.2019.06.038.

[27] A. Enfedaque, M.G. Alberti, J.C. Gálvez, J.S. Proaño, Assessment of the post-cracking fatigue behavior of steel and polyolefin fiber-reinforced concrete, Materials 14 (2021) 7087, https://doi.org/10.3390/ma14227087.

[28] F. Germano, G. Tiberti, G. Plizzari, Post-peak fatigue performance of steel fiber reinforced concrete under flexure, Mater. Struct. 49 (2016) 4229–4245, https://doi.org/10.1617/s11527-015-0783-3.

[29] S. Goel, S.P. Singh, P. Singh, Fatigue analysis of plain and fiber-reinforced self-consolidating concrete, ACI Mater. J. 109 (5) (2012) 573–582.

[30] B. Isojeh, M. El-Zeghayar, F.J. Vecchio, Fatigue resistance of steel fiber-reinforced concrete deep beams, ACI Struct. J. 114 (5) (2017) 1215–1226, https://doi.org/10.14359/51700792.

[31] M.K. Lee, B.I.G. Barr, An overview of the fatigue behaviour of plain and fibre reinforced concrete, Cem. Concr. Compos. 26 (4) (2004) 299–305, https://doi.org/10.1016/S0958-9465(02)00139-7.

[32] A.E. Naaman, M. Hammoud, Fatigue characteristics of high performance fiber-reinforced concrete, Cem. Concr. Compos. 20 (20) (1998) 353–363, https://doi.org/10.1016/S0958-9465(98)00004-3.

[33] A. Nanni, Fatigue behaviour of steel fiber reinforced concrete, Cem. Concr. Compos. 13 (4) (1991) 239–245, https://doi.org/10.1016/0958-9465(91)90029-H.

[34] S.J. Stephen, R. Gettu, Fatigue fracture of fibre reinforced concrete in flexure, Mater. Struct. 53 (3) (2020).

[35] J. Zhang, H. Stang, V.C. Li, "Crack bridging model for fibre reinforced concrete under fatigue tension, Int. J. Fatigue 23 (2001) 655–670.

[36] B. Boulekbache, M. Hamrat, M. Chemrouk, S. Amziane, Flexural behavior of steel fibre-reinforced concrete under cyclic loading, Constr. Build. Mater. 126 (2016) 253–262, https://doi.org/10.1016/j.conbuildmat.2016.09.035.

[37] G. Campione, N. Miraglia, M. Papia, Mechanical properties of steel fibre reinforced lightweight concrete with pumice stone or expanded clay aggregates, Mater. Struct. 34 (4) (2001) 201–210, https://doi.org/10.1007/BF02480589.

[38] A. Carpinteri, A fracture mechanics model for reinforced concrete collapse, in: Proceedings of the IABSE colloquium on advanced mechanics of reinforced concrete, 1981, pp. 17–30.

[39] A. Carpinteri, Stability of fracturing process in RC beams, J. Struct. Eng., ASCE 110 (3) (1984) 544–558, https://doi.org/10.1061/(ASCE)0733-9445(1984)110:3(544).

[40] A. Carpinteri, A. Carpinteri, Hysteretic Behavior of RC Beams, J. Struct. Eng. 110 (9) (1984) 2073–2084.
[41] C. Bosco, A. Carpinteri, Discontinuous constitutive response of brittle matrix fibrous composites, J. Mech. Phys. Solids 43 (2) (1995) 261–274, https://doi.org/10.1016/0022-5096(94)00058-D.
[42] A. Carpinteri, R. Massabò, Bridged versus cohesive crack in the flexural behavior of brittle-matrix composites, Int. J. Fract. 81 (2) (1996) 125–145, https://doi.org/10.1007/BF00033178.
[43] A. Carpinteri, R. Massabò, Continuous vs discontinuous bridged crack model of fiber-reinforced materials in flexure, Int. J. Solids Struct. 34 (18) (1997) 2321–2338, https://doi.org/10.1016/S0020-7683(96)00129-1.
[44] A. Carpinteri, R. Massabò, Reversal in failure scaling transition of fibrous composites, J. Eng. Mech., ASCE 123 (2) (1997) 107–114, https://doi.org/10.1061/(ASCE)0733-9399(1997)123:2(107).
[45] A. Carpinteri, S. Puzzi, The bridged crack model for the analysis of brittle matrix fibrous composites under repeated bending loading, J. Appl. Mech., ASME Trans. 74 (6) (2007) 1239–1246, https://doi.org/10.1115/1.2744042.
[46] A. Carpinteri, F. Accornero, The bridged crack model with multiple fibers: local instabilities, scale effects, plastic shake-down, and hysteresis, Theor. Appl. Fract. Mech. 104 (2019), 102351, https://doi.org/10.1016/j.tafmec.2019.102351.
[47] A. Carpinteri, F. Accornero, Residual crack opening in fiber-reinforced structural elements subjected to cyclic loading, Strength Fract. Complexity 12 (2–4) (2020) 63–74.
[48] F. Accornero, A. Rubino, A. Carpinteri, Ductile-to-brittle transition in fiber-reinforced concrete beams: Scale and fiber volume fraction effects, Mater. Des. Process. Commun. (2020) 1–11, https://doi.org/10.1002/mdp2.127.
[49] A. Rubino, F. Accornero, A. Carpinteri, Post-cracking structural behaviour in FRC beams: Scale effects and minimum fibre volume fraction, in: Proceedings of the FIB Symposium 2021, Lisbon, Portugal, 2021, pp. 622-631.
[50] F. Accornero, A. Rubino, A. Carpinteri, Post-cracking regimes in the flexural behaviour of fibre-reinforced concrete beams, Int. J. Solids Struct. 248 (2022) 111637.
[51] P. Robins, S. Austin, P. Jones, Spatial distribution of steel fibres in sprayed and cast concrete, Mag. Concr. Res. 55 (3) (2003) 225–235, https://doi.org/10.1680/MACR.2003.55.3.225.
[52] V.C. Li, Y. Wang, S. Backer, Effect of inclining angle, bundling and surface treatment on synthetic fibre pull-out from a cement matrix, Composites 21 (2) (1990) 132–140, https://doi.org/10.1016/0010-4361(90)90005-H.
[53] J.M. Alwan, A.E. Naaman, P. Guerrero, Effect of mechanical clamping on the pull-out response of hooked steel fibers embedded in cementitious matrices, Concr. Sci. Eng. 1 (1) (1999) 15–25.
[54] P. Robins, S. Austin, P. Jones, Pull-out behaviour of hooked steel fibres, Mater. Struct. 35 (2002) 434–442, https://doi.org/10.1007/BF02483148.
[55] S. Abdallah, D.W.A. Rees, Analysis of pull-out behaviour of straight and hooked End steel fibres, Engineering 11 (6) (2019) 332–341, https://doi.org/10.4236/eng.2019.116025.
[56] H. Fataar, M. Combrinck, W.P. Boshoff, An experimental study on the fatigue failure of steel fibre reinforced concrete at a single fibre level, Constr. Build. Mater. 229 (2021), 123869, https://doi.org/10.1016/j.conbuildmat.2021.123869.